ISTITUTO NAZIONALE DI FISICA NUCLEARE

LABORATORI NAZIONALI DI FRASCATI

INSTRUMENTS AND METHODS FOR XRF ANALYSIS OF MULTILAYER MATERIALS

Claudia Polese[1,2], Sultan Dabagov[1,3], Adolfo Esposito[1], Marco Ferretti[4], Astrik Gorghinian[1], Dariush Hampai[1], Andrea Liedl[1,5]

[1] *LNF - INFN, Via E. Fermi 40, I-00044 Frascati, Italy*
[2] *DICMA, Univ. Roma "Sapienza", Via Eudossiana 18, Roma, Italy*
[3] *RAS LPI and NRNU MEPhI, Moscow, Russia*
[4] *ITABC - CNR, Via Salaria km 29.300, 00016 Montelibretti, Italy*
[5] *SBAI, Univ. Roma "Sapienza", Via Scarpa, 14, Roma, Italy*

Abstract

In this paper all the research activities carried out till now for the project of the PhD Course in "Materials, Technologies and Complex Industrial Systems Engineering MATISE" (XXVIII cycle) on the development of XRF analysis for the characterization of multilayer objects of cultural interest are illustrated. This project is carried out within the frame of the collaboration between the laboratory XLab Frascati of Laboratori Nazionali di Frascati (INFN) and the Istituto Tecnologie Applicate ai Beni Culturali di Roma (CNR).

1 Introduction

The X-Ray Fluorescence (XRF) analysis is a widely used technique for the characterization of materials: it is fast, quite simple, suitable for in situ analysis, and gives the elemental composition of the studied object. Its capability of giving qualitative and quantitative information on many different materials, in a non-destructive way, makes it particularly suitable to be applied in many different fields: Medicine, Industry, Cultural Heritage [1].

Through suitable calculations, the quantitative composition can be determined too; it is now quite simple in case of homogeneous materials, thanks to the development of various software operating with the Fundamental Parameter method [2–4], allowing to manage all the parameters of the system (X-ray source, detector, geometry of the system, matrix). But when we have to deal with multilayer materials, a particular case of heterogeneous materials, it gets more complicated. The problem is due to the high penetration of X-Rays in the matrix that leads to various layers of different compositions included in the analytical volume, whose individual contributions are not easy to be separately revealed.

There are some proper softwares to process the XRF spectra of this kind of materials too: one of them is PyMCA (Python MultiChannel Analysis) developed at ESRF (European Synchrothron Radiation Facility, Grenoble) [5]. Further than the usual accurate description of the measurement system (X-Ray source, primary beam, detector, geometry of the system), it allows up to 10 layers of the matrix to be described, each one with its own hypothetical density, thickness and composition, as well as their fluorescence contributions to be unfolded.

In literature some examples of its employment are already available [6], applied to different materials like paintings [7], gilded [8] and enameled metals [9]. In the case of a two-layered materials, a gilded silver, where the substrate can be thought of infinite thickness, we can determine the thickness of the upper layer relying on the dependence of the intensity ratio AgKα/AgKβ on the coating thickness. PyMCA can calculate Ag concentrations separately on AgKα and AgKβ, so the gilding thickness (t_g) can be determined by imposing the condition:

$$C_{AgK\alpha}(t_g) = C_{AgK\beta}(t_g) \tag{1}$$

The thickness parameter in the PyMCA configuration is iteratively corrected until this condition is fulfilled.

Once the gilding thickness is determined, the quantitative analysis of both layers becomes possible. This method gives a good reliability for the gilded metals, while for the glass matrices is more fragile. Because of the instrumental and physical limits in detecting the light elements, such as Si and Na, which are principal components of both glasses and enamels, the matrix approximation in the PyMCA configuration is less real-

istic, and leads to a considerable error on the thickness determination, too. Furthermore, the current versions of PyMCA does not take into account the secondary fluorescence effect, quite important in glass matrices [10,11], generating other errors on the quantitative determination.

Using a normal XRF system, the incident beam size is too big (around 1 mm^2) for the analysis of very little areas, such as in not homogeneous deteriorated surfaces of archaeological objects or finely enameled metal plates, where the analytical volume comprises close areas of different composition, leading again to a complication in the quantitative determination.

This project aims at the improvement of a spatial resolution of XRF system in order to carry out in situ micro-analysis, too, by polycapillary lenses [12–15]. This kind of optics, one of the efficient in focusing X-rays, can produce high intensity beams thanks to the peculiars geometry.

A polycapillary lens consists of many hollow glass channels (each working as a waveguide) arranged in a barrel shape (in reality, the shape is variable): it collects a great solid angle and, deviating the photons by multiple reflections inside every channel, focuses the beam in a small spot with a higher density radiation respect to a simple pinhole. For glancing angles smaller than the critical angle θ_c, the incident photon is reflected from the internal channel walls by Total External Reflection (TER), as in the X-ray energy range the air has the higher refraction index. The θ_c value is inversely proportional to the incident beam energy, as can be seen in the following equation:

$$\theta_c \approx (\hbar\omega_p)/E \qquad (2)$$

where E is the energy of the incident photon, $\hbar$ is the Planck costant, and ω_p is the plasmon frequency of the reflecting surface. It means that, when dealing with X-rays, the geometry of the system must assure an incident angle smaller than 1°, with clearly technological difficulties.

Polycapillary optics have been already used in some μ-XRF systems (e.g. Unisantis products): the challenge is to combine them with a XRF system suitable for the detection of K-lines of heavy elements such as Ag, Sn, Sb, Ba and Cd., very important in Cultural Heritage materials, for example enameled metals. It could be not so easy because, as already said, the photon energies greatly influence the geometrical design of the optics, leading to manufacturing complications, and we will need a polycapillary capable to focus an X-ray beam energetic enough to excite fluorescence K-lines above the 20 keV.

The second goal is to improve the quantitative analysis of XRF spectra, by integrating the PyMCA software into the Monte Carlo simulations code (XMI-MSIM) [16]

3

to adjust the results for the secondary fluorescence effects. In such way we could obtain better results especially for glass matrices, but also refine the already good data on metals.

In this paper we report all the experimental activities carried out until now, in order to reach our proposed goals:

- Alignment procedures for polycapillary lenses;
- Characterization of focusing lenses and shaped by them beams;
- Beam filtering;
- XRF measurements with a focusing lens on gilded and enameled silver standards;
- Data processing, by the PyMCA software and Monte Carlo simulation, of XRF spectra of silver and copper alloys.

2   Experimental Setup

As X-ray source we used two different tubes. For the measures related to the polycapillary optics we used one of the X-ray tube Oxford Apogee at XLab Frascati of INFN-LNF, where the measurements were carried out: it is a W anode, voltage 50 kV. For the direct measures of the primary beam and to test the filters, we use a current ~ 1 μA to avoid damages to the detector, because a flux too intense would have broken it, while for XRF measured on the standards we set it to 1 mA to have a fluorescence signal intense enough. For the filtering tests we used some filters of steel (Fe 74%, Cr 18%, Ni 8%) of 35 μm thickness and others of copper of 30 μm thickness. For the XRF measures related to the Monte Carlo testing, we used another Oxford X-ray tube, at ITABC-CNR laboratories: it is a W anode, voltage 60 kV and current 1.5 mA, with an internal filter of copper of 300 μm, a beam size ~ 1 mm^2, and a two lasers pointing system.

For the detection of XRF spectra we used two different Bruker Si-Drift Detector of the ITABC-CNR. The first one has an active area 10 mm^2, thickness 450 μm, FWHM 175 eV at 5.9 keV, peaking time 1 μs, beryllium window, internal zirconium collimator, and an external lead collimator for the direct measures. The second one is similar, but with an active area 30 mm^2 and an internal collimator of molybdenum. The time acquisition was 120 seconds.

The polycapillary optic is a focusing lens with input focal distance (IFD) 56.5 mm, output focal distance (OFD) 44 mm, length 12 cm, and the diameter of output focal spot size is 100 μm.

The polycapillary system was put in a security chamber and for the spatial scanning we use a set of Newport motors and holders, controlled with a Newport MM4006 Controller by a Labview software.

For the alignment measurements we used a scintillator Ortec 3 KV, and for the

determination of the OFD and the beam size we used a camera CCD Photonic Science FDI 1:1.61 with the software package Image-Pro Plus 6.0: active area of 14.4 x 10.8 mm^2 with a resolution of 10.4 x 10.4 μm^2.

Table 1: Gilded silver standards. The gilding thickness was verified at ENEA by a surface palpator (on the samples are visible the signs of the measures, leaving an uncovered silver band).

ID	Std1	Std2	Std3	Std4	Std5	Std6
Image						
Gilding thickness (μm)	1.967	2.700	4.143	4.440	5.780	7.300

Table 2: Nominal composition of standard materials.

a. Silver alloys

ID	Cu%	Au%	Ag%
ICR1	2	0	98
ICR2	6	0	94
ICR4	2	2	96
ICR5	2	6	92
ICR6	6	2	92
ICR7	6	6	88
ICR8	10	2	88
ICR9	10	6	84
INFN1	2	0	98
INFN2	4	0	96
INFN3	10	0	90
INFN4	15	0	85
INFN5	12	2	86
INFN6	9	4	87
INFN7	5	6	89
INFN8	3	10	87
INFN9	1	1	98
INFN10	0	8	92

b. Copper alloys

	SS551	SS552	SS553	SS555	SS556
Si %	0.018	0.019	0.022	0.005	0.005
P %	1.01	0.77	0.68	0.18	0.1
Fe %	0.2	0.1	0.056	0.01	0.004
Ni %	0.76	0.56	0.44	0.11	0.014
Cu %	87.4	87.7	87	87.1	86.4
Zn %	0.74	0.35	0.49	0.09	0.09
Sn %	8.92	9.78	10.8	12.1	13.2
Pb %	0.7	0.63	0.47	0.24	0.16

For the quantitative analysis we used the latest version of PyMCA (4.7.RC5), a new prototype with the plug-in XMI-MSIM for the Monte Carlo simulations.

For the XRF analysis on multilayer objects we used some reference materials: 6 standards of silver sheets (Ag925% with Cu traces, 1 mm thick) with different gilding thicknesses (tab.1), obtained by sputtering at Laboratorio di trattamento e deposizione Film sottili of ENEA, and another silver substrate of same composition to estimate the

incident flux; an enameled silver standard (same substrate) realized with the cloisonn technique (enamel thickness: 0.99 mm) at Scuola dellArte della Medaglia dellIstituto Poligrafico e Zecca dello Stato (SAM - IPZS). For the Monte Carlo testing, we used a set of reference samples of silver and copper alloys (tab.2).

3 Experimental activities

3.1 Alignment procedures for polycapillary lenses

The procedure to align a polycapillary optic with the X-ray source, to obtain the best transmission, is well described in [17]. When the input focal distance is known (in this case 56.5 mm from the focus of the tube), the input side of it can be fixed by an holder, while with two motors we scan the two angular coordinates to correct the inclination respect to the beam direction (fig.1). For every angular position, the intensity of transmitted radiation is measured with a scintillator: the optimal position is the one with the maximum counting rate. The entire system is automatized and can be controlled by a LabView software.

When the input focal distance is unknown, the procedure has to be repeated with a further scanning of the distance tube-lens: at every step of the latter scanning the normal alignment procedure has to be done, so that we can compare the maximum intensity of every step and find the right distance.
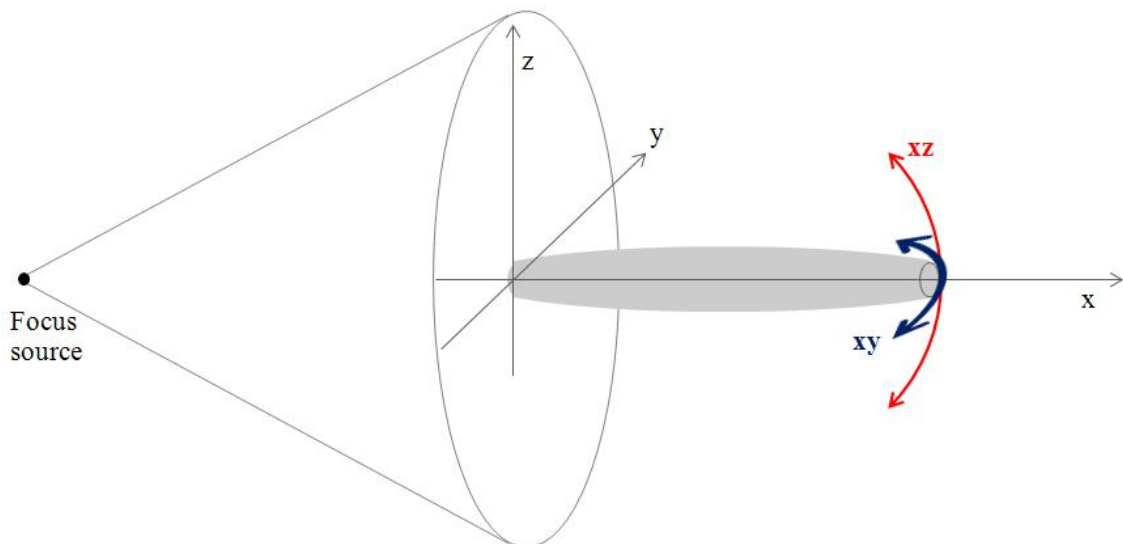

Figure 1: Scheme of a scanning system of the lens: the input side in the origin is fixed, while the lens is moved along two orthogonal planes (xy and xz).

3.2 Characterization of focusing lenses and their focused beam

Once aligned a lens, to determine its output focal distance (OFD) we took some images with the CCD camera, at various distance from its exit (fig.2, fig3, tab.3), for an acquisition time of 200 ms: the focus is the distance at which the beam spot is smaller, and consequently more intense. In this way we can also measure the beam size. The tube was setted at ~ 43.5 kV and ~ 4 μA. In fig3 we can easily recognize picture 3 as the one corresponding to the closer value to the real OFD.

Figure 2: Scheme of a CCD camera image acquisition system, at various distances from the lens output.

Table 3: Distance of measurements from the lens.

ID	1	2	3	4	5	6	7	8	9	10
Distance from the lens (mm)	36	41	46	51	56	61	66	71	76	81

Figure 3: Set of images taken with the CCD at various distances: the picture 3 shows the better focused beam.

In order to characterize the beam coming out from the focusing lens, which is different from the one produce by the source [14], we carried out some direct measure putting the SDD Detector (the one with active area 10 mm^2) in front of the tube, with and without

the polycapillary lens, for an acquisition time of 120 seconds. We set the current of the tube at its minimum ($\sim 1~\mu$A) to reduce the flux, and put the detector far from the lens focus (at 39 cm from its exit), in order to avoid damages to the detector due to a too intense signal. Measuring the beam is important to understand how much the lens change the original one, and if it will be able to excite fluorescence K-lines at high energies. Registering the primary beam will be useful also in a second time, to do the quantitative analysis by the Fundamental Parameter method, as we need to give to the software the incident weighted energies [2].

For the FP method, we need to know the real primary beam that will impinge on the sample surface, which is not the one measured by the detector: we have to correct it by the detector efficiency, which decrease exponentially with the incident energies, with the following equation [1,2]:

$$C_{corrected}(i) = \frac{C(i)}{1 - e^{-\mu(E)\rho x}} \tag{3}$$

where C(i) are the counts measured for every channel or energy; μ, ρ and x are respectively attenuation coefficient, density and thickness of the silicon detector.
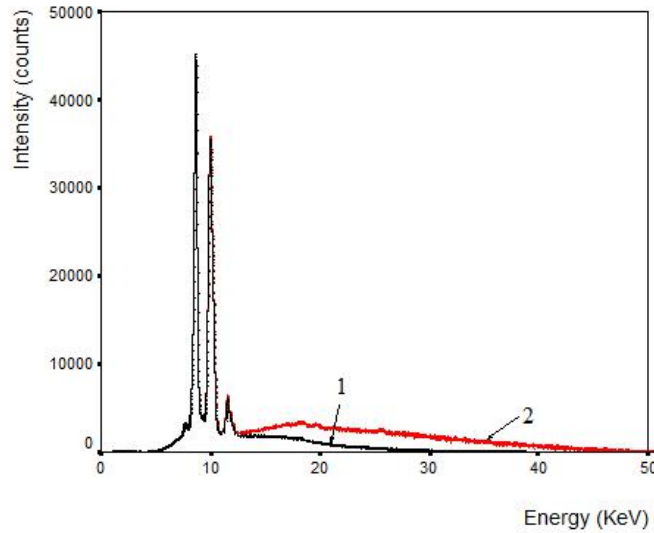

Figure 4: Comparison of the measured spectrum (black, 1) and the corrected one (red, 2): they are referred to a measure without the polycapillary lens, of the primary beam.

Watching at fig.4 becomes evident why correcting the measured beam is necessary: it changes a lot in the high energy region. In fig.5 the spectra measured with and without the lens at the same distance from the source are compared. The spectra are normalized so that the sum of the counts is 1: in the smaller graph there are the real intensities too, to show that although in the normalized ones it seems that the lens spectrum has

8

more intense W-L lines, this is not true, because the global intensity of the spectrum is greatly reduced. In the primary spectrum we can see the bremsstrahlung and the L-lines of tungsten: the K-lines of the anode (> 60 keV) are not excited because of the low voltage (50 kV). Comparing them it is possible to see how the polycapillary lens reduces the bremsstrahlung component at high energies and shifts its maximum at lower values.
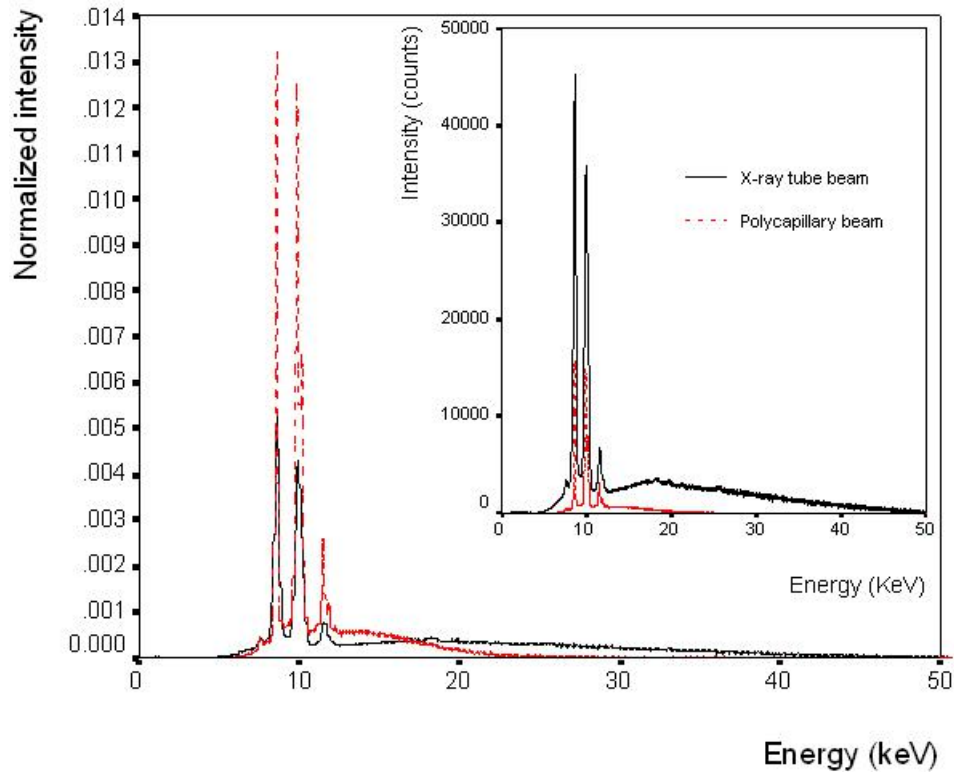

Figure 5: Spectra of X radiation of the tube without (black continuous) and with (red dashed) the lens: both of them have been taken at the same distance, and the spectra areas have been normalized to 1. In the smaller graph the same spectra, corrected for the detector efficiency, are illustrated with the real intensity values.

3.3 Beam filtering

Once characterized the primary beam, we tried to optimize it for the analysis of metals and glasses, by the enhancement of the high energy fraction. We tested some filters of different composition, placed between the source and optics to cut off the L-lines of tungsten, always by direct measurements. We first try a steel filter, that cut off only the lower energy lines, and then we add also a copper filter, obtaining a good result (fig.6, tab.4). The optimum solution is the employment of two filters of both steel and copper.

9

These spectra were then discretized in 50 weighted values in order to be used by PyMCA for the quantitative analysis.

Table 4: In this table the fluorescence (W)L-lines energies are shown, together with the absorption edge values of the elements present in the filters used (tabulated in PyMCA).

Fluorescence line	Energy (keV)	Filter element	Absorption edge (keV)
W Lα1	8.4	Ti	5
		Cr	6
		Fe	7.2
W Lβ2	9.7	Cu	9
W Lγ3	11.28		
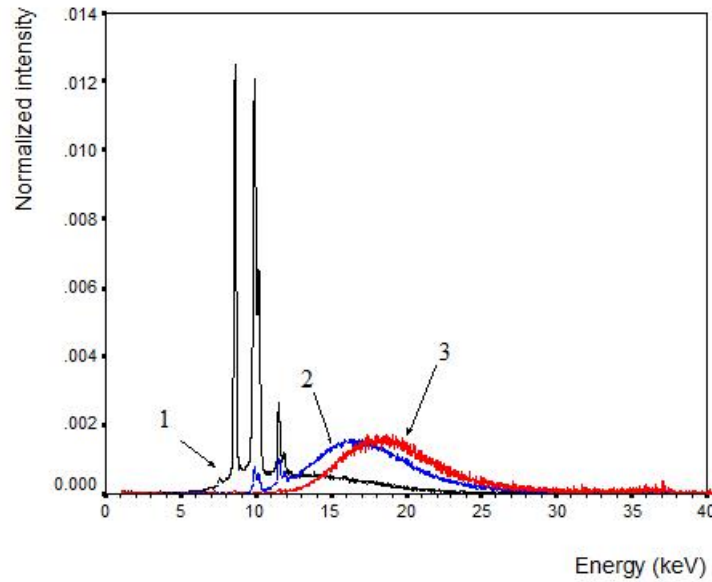
Figure 6: Spectra of the lens (black, 1), with a steel filter (blue, 2) and with steel + copper filters (red, 3): the spectra areas have been normalized to 1 (this is why the filtered beams appear more intense than the not filtered one).

3.4 XRF measurements with a focusing lens on gilded and enameled silver standards

To verify the efficiency of the beam, filtered and focused as before mentioned, in the excitement of silver fluorescence K-lines, we carried out a set of measures on 6 standards of gilt silver and on an enameled silver standard. This time the current of the XLab tube

10

was 1 mA, and the external lead collimator was removed. The incident angle was 90° and the take-off angle 45° (fig.7).

First of all we compared qualitatively the XRF spectra obtained in this way with the ones measured with a similar set-up, but different tube (the CNR-ITABC one), without polycapillary optics.

With the latter configuration the primary beam has a greater high energy fraction, and allows a more efficient excitation of silver K-lines. Although these measures are conducted in clearly better conditions, fig.8 and fig.10 show that the use of an optic gives a good excitation of silver K-lines from the substrate, too.
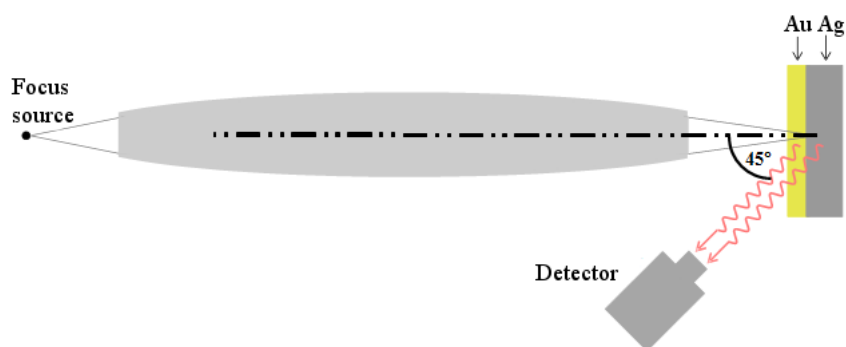
Figure 7: Geometry of XRF acquisition system.

a.   b.
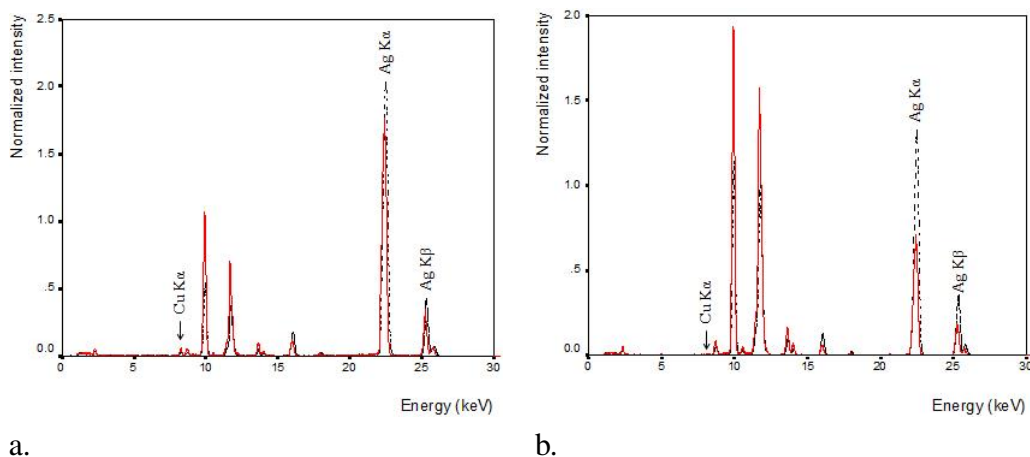
Figure 8: XRF spectra of Std1 (a) and Std6 (b) with (red continuous) and without (black dashed) the polycapillary lens; the spectra areas have been normalized to 1.

On the other hand, with the polycapillary set up there is a problem in the count rate, due to the fact that the filtering of the beam allows the use of only the high energy fraction transmitted by the lens. This problem is evident especially in the detection of copper in the substrate, for gilding thickness over 5 μm (fig.8).
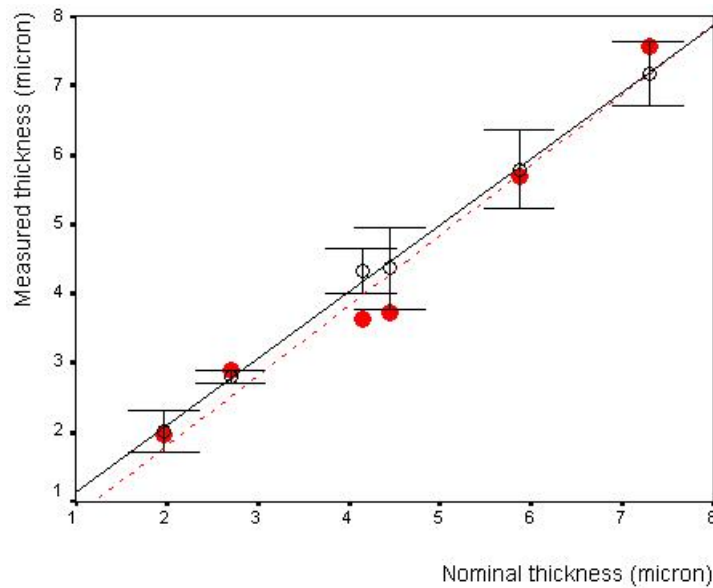
11

Figure 9: Gilding thicknesses measured for XRF spectra with (red, full circles) and without lens(black, with the standard deviation bars).

The XRF spectra have then been processed by PyMCA software with the method described before [9] to determine the gilding thickness, in order to verify if the counts on silver K-lines can give reliable results.

At a first comparison between the results obtained in the two different ways (fig.9), the method seems reliable also with the polycapillary set up. For the run with the polycapillary, we have only one value for each standard, and we cannot still determine the error of the method because we could not use any pointing system, so we do not know if the error (especially in the case of the thickness around 4 μm) is the uncertainty of the method or is due to the a wrong sample positioning: the results could be improved, whereas a pointing system of the beam will be available for the polycapillary configuration too.

Looking at the XRF spectrum of the enameled silver (fig.10), a good excitation of silver substrate K-lines and the other elements by the polycapillary system can be seen, but is also evident the lower excitation of the barium in the upper enamel layer, which leads to its great overestimation in the quantitative analysis. The spectrum of the enameled silver is compared to the one obtained with the CNR-ITABC configuration, and also with another similar one, which uses an helium flux (by the application of a He collimator on the detector head), in order to improve the detection of light elements as potassium. In the smaller graph is possible to see how the polycapillary lens gives the better signal-to-noise ratio for the K-line of potassium, which is at the lower detection limit.
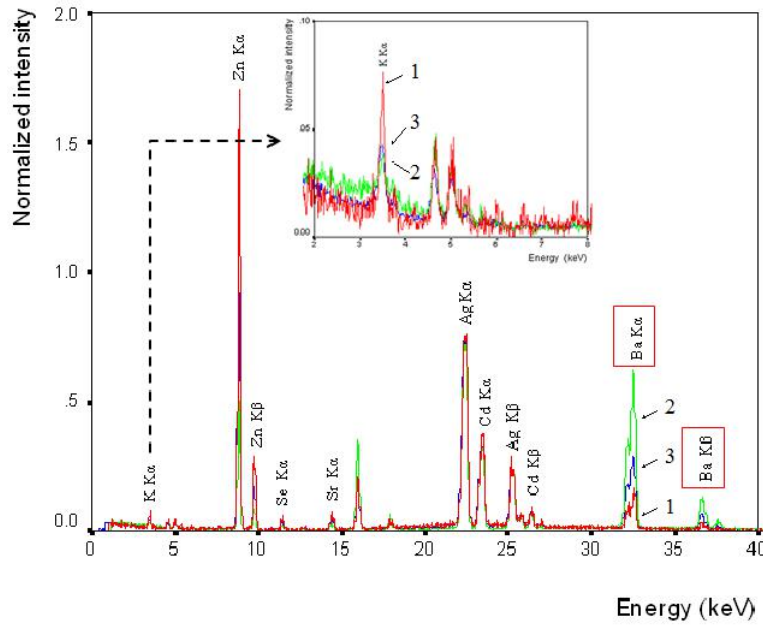
Figure 10: XRF spectra of enameled silver standard, with the polycapillary lens (red, 1), the reference configuration (green, 2) and in helium flux (blue, 3); the spectra areas have been normalized to 1. In the zoomed graph, we can see the different signal-noise ratio for the (K)Kα.

3.5 Data processing, by both PyMCA software and Monte Carlo simulation, of XRF spectra of both silver and copper alloys

To evaluate if and how much the Monte Carlo simulation could improve the accuracy of the quantitative analysis performed by PyMCA, we carried out 5 series of XRF measures on some standard of silver and copper alloys, for an acquisition time of 120 seconds with the CNR-ITABC tube. On the silver alloys the detector with active area 10 mm^2 was

Table 5: Average relative error on majority elements of the standard alloys, obtained with (MC) and without Monte Carlo (PyMCA).

a. Silver alloys		
	PyMCA	MC
Cu	27 %	15 %
Au	27 %	12 %
Ag	51 %	12 %

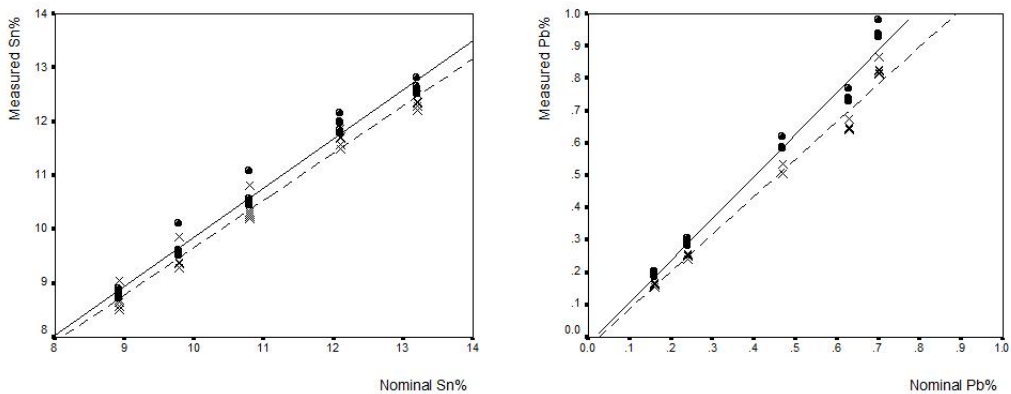| a. Copper alloys		
	PyMCA	MC
Fe	1185%	430%
Ni	914%	627%
Cu	33%	14%
Zn	294%	230%
Sn	2.4%	4.2%
Pb	24%	8%

used, while for the copper alloy the one of 30 mm^2; we processed the XRF spectra both with and without the Monte Carlo plug-in.

13

The results for the silver alloys, where the secondary fluorescence effect is important (Cu K-lines are excited from Ag K-lines), if treated with the Monte Carlo show an average deviation which is almost 50% less than without it (tab. 5.a, fig.11).
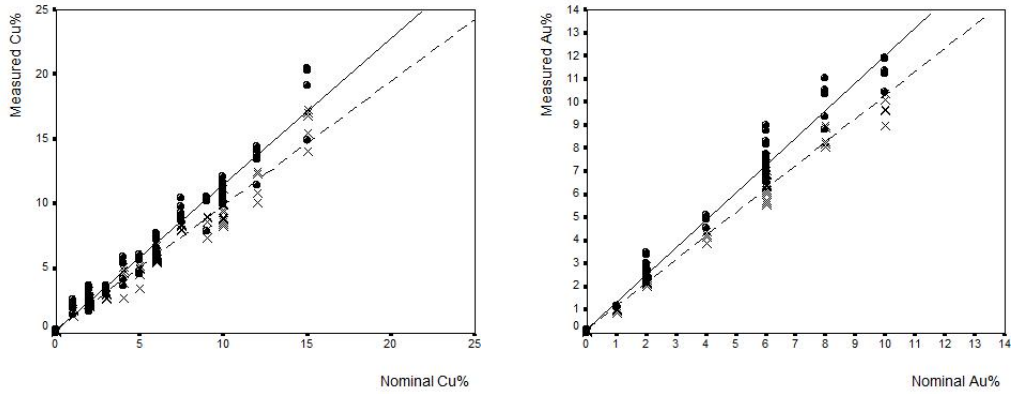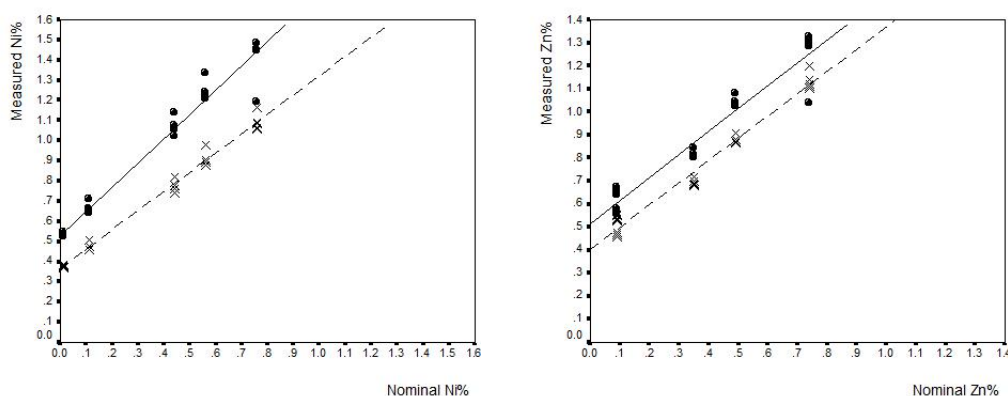

a.   b.

Figure 11: Comparison between the Cu% (a) and Au% (b) measured and nominal values, for silver alloys, with (x) and without (circles) Monte Carlo.

As regards the copper alloys, the improvement is less evident (also because of the peculiar composition of the standards, that does not let appreciate the effect), but it is still present (tab. 5.b): in particular, there are good results on tin (fig.12.a), lead (fig.12.b) and copper, the major element. The Monte Carlo correction can adjust the lead content, which suffers secondary fluorescence from tins K-lines, and reduces deviations on iron, nickel and zinc (fig.13), although they still systematically remain above the nominal values.

a.   b.

Figure 12: Comparison between the Sn% (a) and Pb% (b) measured and nominal values, for copper alloys, with (x) and without (circles) Monte Carlo.

Figure 13: Comparison between the Ni% (a) and Zn% (b) measured and nominal values, for copper alloys, with (x) and without (circles) Monte Carlo.

4 Conclusion

Looking at these preliminary results, it seems that tested focusing polycapillary lens could be suitable for XRF analysis of a gilded silver object, because it gives a sufficient excitation of Ag K-lines of the substrate, although more tests will be necessary to evaluate the uncertainty of the thickness determination method. As regards the enamels, further investigations should be done to implement the system capability of exciting elements as barium in a proper way, although on the other hand the polycapillary configuration seems the more efficient in the detection of very light elements as potassium.

It is clear how the use of a very small incident beam represents both a problem of representativeness of the single measure (on areas very much smaller than the entire object), and an advantage because, for example, it allows small areas naturally without patinas of a heterogeneously deteriorated object to be analyzed, avoiding any further invasive action.

Referring to the Monte Carlo contribution to the quantitative analysis, the first results obtained make us quite optimistic in its use, and next step is to apply it on the glass matrices with a more complex composition, which will require more time for each running of the software, as a bit time-consuming method is. It is still inadequate in the case of great set of measures, as it cannot be applied by batching fits.

5 Acknowledgements

We are grateful to:

- Dr. Fiorenzo Catalli (Director of Monetiere di Firenze) for ospitality at Palazzo

15

Altemps - Museo Nazionale Romano.

References

[1] P. Moioli *et al*, Fluorescenza X. Prontuario per l'analisi XRF portatile applicata a superfici policrome (Firenze, 2002).

[2] R. Jenkins *et al*, Quantitative X-Ray Spectrometry (2nd ed.), (MarcelDekker Inc., New York, 1995).

[3] D.K.G. De Boer, X-Ray Spectrometry **19**, 3 (1990), p. 145.

[4] D.W. Marquardt, Journal of the Society for Industrial and Applied Mathematics **11**, 2 (1963), pp. 431-441.

[5] V.A. Sol *et al*, Spectrochimica Acta Part B **62** (2007), pp. 63-68.

[6] K. Nygard *et al*, X-Ray Spectrometry **33** (2004), pp. 354-359.

[7] L. De Viguerie *et al*, Angewandte Chemie International Edition **49** (2010), pp. 1-5.

[8] R. Cesareo *et al*, Nuclear Instruments and Methods in Physics Research B **267** (2009), pp. 2890-2896.

[9] M. Ferretti *et al*, Spectrochimica Acta Part B **83-84** (2013), pp. 21-27.

[10] A.G. Karydas, X-Ray Spectrometry **34** (2005), pp. 426-431.

[11] L. Bonizzoni *et al*, X-Ray Spectrometry **29** (2000), pp. 443-448.

[12] S.D. Dabagov, Physics - Uspekhi **46**, 10 (2003), pp. 1053-1075.

[13] M.A. Kumakhov *et al*, Physics Reports (Review Section of Physics Letters) **191**, 5 (1990), pp. 289-350.

[14] P.J. Schields *et al*, Powder Diffraction **17**, 2 (2002), pp. 70-80.

[15] N. Gao *et al*, Polycapillary X-ray Optics, in: X-Ray Spectrometry: Recent Technological Advances (K.Tsuji *et al*, 2004), pp. 89-110.

[16] T. Schoonjans *et al*, Spectrochimica Acta Part B **82** (2013), pp. 36-41.

[17] G. Cappuccio *et al* Proc. SPIE **4155** 40 (Kumakhov Optics and Application, 2000).